CrystEngComm

Cite this: *CrystEngComm*, 2012, **14**, 4618–4624

www.rsc.org/crystengcomm

PAPER

Highly uniform $NaLa(MoO_4)_2$:Ln^{3+} (Ln = Eu, Dy) microspheres: template-free hydrothermal synthesis, growing mechanism, and luminescent properties†

Zuoling Fu,*[ab] Wanwan Xia,[ab] Qisong Li,[ab] Xiaoyun Cui[ab] and Wenhao Li*[c]

Received 15th December 2011, Accepted 28th March 2012
DOI: 10.1039/c2ce06682c

Uniform and well-crystallized $NaLa(MoO_4)_2$ microspheres were prepared by a facile one-step hydrothermal synthesis without involving any surfactants or templates. The as-obtained products were systematically characterized by powder X-ray diffraction (XRD), field emission-scanning electron microscopy (FE-SEM), transmission electron microscopy (TEM), photoluminescence (PL), and photoluminescent excitation spectra (PLE). The influence of the starting pH value on the phase and morphology of $NaLa(MoO_4)_2$ microspheres was discussed. Furthermore, the formation mechanism of the microspheres was dominated by the consequence of a fast crystallization, dissolution and recrystallization. Finally, the luminescent properties of Eu^{3+} and Dy^{3+} ion activated $NaLa(MoO_4)_2$ microspheres were investigated. The results demonstrated that $NaLa(MoO_4)_2$:Ln^{3+} (Ln = Eu, Dy) microspheres exhibited good luminescent properties and might have potential applications in lighting technology.

1. Introduction

The synthesis of micro- and nanoscale inorganic materials with a special size and morphology, including hierarchical structures, have gained much attention due to their fundamental scientific interest and potential technological applications in different fields such as photochemistry, superconductors, optoelectronics, solar cells, and catalysis.[1–3] Therefore, the tunable or controllable morphology of nano/microcrystals remains an important goal of modern materials chemistry. Many recent efforts have been devoted to the controllable morphology and spatial patterning of various materials, which is a crucial step toward the realization of functional nanosystems.[4–7] Generally, for obtaining different morphologies, chemical vapor deposition or solution-phase chemical routes have been used; however, they usually require catalysts, expensive and even toxic templates or surfactants, high temperature, and a series of complicated procedures. Therefore, it is still a big challenge to develop simple and reliable synthetic methods for hierarchical architectures with designed chemical components and controlled morphologies, which strongly affect the properties of nano/micromaterials.

Double alkaline rare-earth molybdates and tungstates ($ALn(MO_4)_2$, where A = K, Na, Ln = La, Y, and M = Mo, W) form a wide variety of inorganic compounds having tetragonal and monoclinic symmetries. Their structural diversity provides numerous physical properties. It is well known that the rare-earth-doped materials including phosphors have a wide variety of applications for their use in the development of solid state lighting, display systems, scintillators,[8] laser,[9] and amplifiers for fiber-optic communication.[10] Over a long time the investigations on the $ALn(MO_4)_2$ family of compounds are concentrated on the laser properties of single crystals pf $ALn(MO_4)_2$ with small grain sizes while other uses have received little attention. Recently, it has been realized that the powder samples of this family might be promising candidates as phosphors for visual display[11] and solid-state lighting.[12] However, to the best of our knowledge, the reports focused on the synthesis and optical properties of rare-earth-doped $ALn(MO_4)_2$ are still limited. Also, most of the synthesis reports on these materials remain in the stage of solid phase synthesis or high temperature liquid synthesis.[13–16] These approaches usually require high temperatures, time-consuming heating processes and subsequent grinding. The grinding process damages the phosphor surfaces, resulting in the loss of emission intensity.[17,18] In addition, the aggregation and in-homogeneous shapes are also unavoidable, which inhibit the absorption of the excitation energy and therefore reduce the emission intensity.

Recently, the template-free hydrothermal technique has been considered as a promising method for the synthesis of some inorganic powders owing to the flexible conditions including simplicity of equipment and processing, low reaction temperature, and desirable reaction conditions. Therefore, using the

[a]*State Key Laboratory of Superhard Materials, College of Physics, Jilin University, Changchun, 130012, China. E-mail: zlfu@jlu.edu.cn; Fax: 86-431-85167966; Tel: 86-431-85167966*
[b]*Key Lab of Coherent Light, Atomic and Molecular Spectroscopy, Ministry of Education, Changchun, 130012, China*
[c]*Changchun Institute of Optics, Fine Mechanics and Physics, Chinese Academy of Sciences, Changchun, 130033, China. E-mail: leewenho@163.com*
† Electronic Supplementary Information (ESI) available. See DOI: 10.1039/c2ce06682c/

hydrothermal synthesis, it is possible to obtain a homogeneous composition with uniform morphology and phase with stable physical properties.[19] In this paper, we report the controlled synthesis of $NaLa(MoO_4)_2$ microspheres *via* a simple hydrothermal process without using any templates, surfactant, other organic additives, and further calcination treatment. The optimal synthesized conditions for $NaLa(MoO_4)_2$ microspheres were studied and the phenomenological formation mechanism for the microspheres was discussed. Finally, the luminescent properties of Eu^{3+} and Dy^{3+} ion doped $NaLa(MoO_4)_2$ microspheres were investigated.

2. Experimental

2.1. Synthesis of the samples

Materials. All reagents from the Beijing Chemical Company were analytical grade, and used directly without further purification. The ammonium molybdate tetrahydrate ($(NH_4)_6Mo_7O_{24}\cdot4H_2O$) was used as the molybdenum source, lanthanum nitrate hexahydrate ($La(NO_3)_3\cdot6H_2O$) as the lanthanum source, and sodium hydroxide (NaOH) as the sodium source. Meanwhile, europium nitrate pentahydrate ($Eu(NO_3)_3\cdot5H_2O$) and dysprosium nitrate hexahydrate ($Dy(NO_3)_3\cdot6H_2O$) offered the europium and dysprosium source, respectively. For the hydrothermal treatment, we used 60 mL Teflon cups.

Synthesis. In a typical procedure 0.57 mmol of $(NH_4)_6Mo_7O_{24}\cdot4H_2O$ and 2 mmol $La(NO_3)_3\cdot6H_2O$ were dissolved in 20 mL distilled water to form an aqueous solution, and then mixed together with strong magnetic stirring at room temperature for 10 min to form a homogeneous solution. Next, the same solutions were adjusted to the desirable pH values (4, 5, 6, 7, 8, 9, 10) by adding drop wise into the above solutions a desired amount of NaOH (5 M) under vigorous stirring before hydrothermal treatment, respectively. The amount of NaOH added was controlled by the pH value showing on the pH-meter (the Micro-Digit PH/mv Meter with high accuracy of ±0.01 pH), assisted by adding drop wise diluted HNO_3 solution when it was necessary. Firstly, NaOH immediately reacted with the molybdenum source and rare earth nitrate solutions, and a slurry-like white precipitate was formed. The mixture was stirred again for 1 h. Finally, the mixture was placed in a polytetrafluoroethylene (PTFE) vessel, and the vessel was capped by a PTFE cover and placed inside a stainless steel autoclave. The autoclave was maintained at 180 °C for 12 h and cooled naturally to room temperature. The precipitate was filtered and washed with alcohol and deionized water several times. The final products (about 1.4 mmol) were dried at 60 °C for 12 h in air. $NaLa_{1-x}(MoO_4)_2{:}xLn^{3+}$ (Ln = Eu or Dy) samples were synthesized in the same flow path.

2.2. Characterization

Powder X-ray diffraction (XRD) measurements were performed on a Rigaku-Dmax 2500 diffractometer with Cu-Kα radiation (λ = 0.15405 nm). The morphology and structure of the obtained samples were inspected using a field emission-scanning electron microscope (FE-SEM, XL30, Philips) and transmission electron microscopy (TEM, JEM-2010 JEOL).

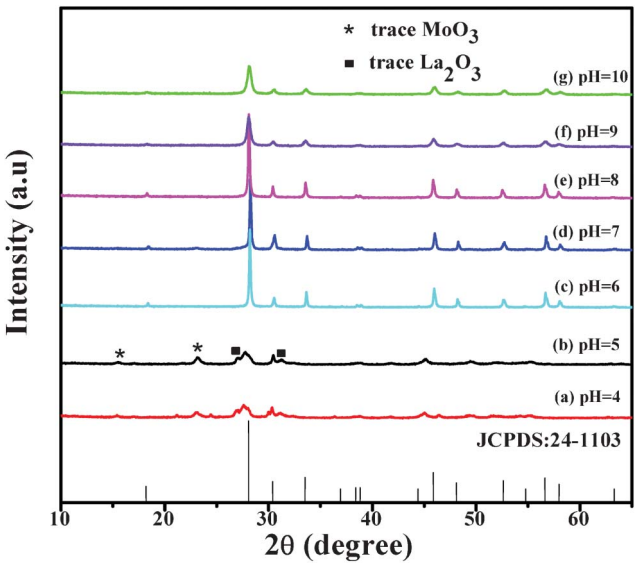

Fig. 1 XRD powder patterns of $NaLa(MoO_4)_2$ samples prepared by hydrothermal method at 180 °C for 12 h at (a) pH = 4; (b) pH = 5; (c) pH = 6; (d) pH = 7; (e) pH = 8; (f) pH = 9; (g) pH = 10.

The ultraviolet-visible photoluminescence (PL) excitation and emission spectra were recorded with a Hitachi F-7000 spectrophotometer equipped with a Xe lamp as an excitation source. All the measurements were performed at room temperature.

3. Results and discussion

3.1. Phase formation, structure, and morphology of $NaLa(MoO_4)_2$ samples

Fig. 1 shows the XRD patterns of $NaLa(MoO_4)_2$ samples obtained at 180 °C for 12 h under different pH values. A suitable pH value for the synthesis of single phase crystalline $NaLa(MoO_4)_2$ powders was investigated by varying the base (NaOH) concentration. The XRD results revealed that the pH values of the reaction solution played an important role in controlling the phase structures. When the value of pH $\leqslant$ 5, traces of MoO_3 and La_2O_3 appeared as impurity peaks (Fig. 1(a) pH = 4 and (b) pH = 5). Whereas beginning with pH = 6, no impurity peaks were detected in this experimental range (Fig. 1(c)). All of the diffraction peaks can be indexed to the scheelite-type tetragonal structure (JCPDS No. 24-1103) with $I4_1/a$ lattice symmetry. The lattice constants were calculated to be $a = b = 5.343$ Å and $c = 11.743$ Å. The tetragonal phase of $NaLa(MoO_4)_2$ remained when the pH value was controlled in the range from 7 to 8 (Fig. 1(d) pH = 7 and (e) pH = 8). In addition, the strong and sharp diffraction peaks indicated a good crystallinity of the resulted samples. Further increasing the pH up to 9–10, the diffraction peaks of the samples became weak and broad due to the decreased crystallinity (Fig. 1(f) pH = 9 and (g) pH = 10). These results indicate that pure and well-crystallized $NaLa(MoO_4)_2$ samples can only be obtained in an appropriate pH range of 6–8, which are in good accordance with the observed FE-SEM images shown in Fig. 2.

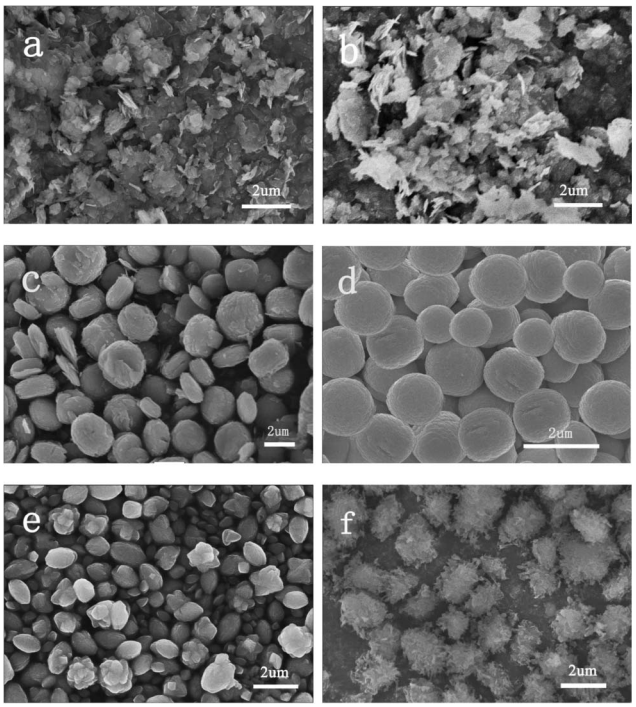

Fig. 2 FE-SEM images of $NaLa(MoO_4)_2$ crystallites prepared hydrothermally at 180 °C for 12 h at (a) pH = 4; (b) pH = 5; (c) pH = 6; (d) pH = 7; (e) pH = 8; (f) pH = 9.

To fully understand the effect of pH value on the microstructure and morphology of the synthesized samples, controlled experiments were conducted to find the optimal morphology. Fig. 2 shows the morphology evolution of resultant $NaLa(MoO_4)_2$ crystallites from different starting pH values after hydrothermal treatment at 180 °C for 12 h. It indicates that the morphology of $NaLa(MoO_4)_2$ crystallites can be tailored by adjusting the pH value of the suspension solution. When pH = 4 (Fig. 2a), the micrographs reveal the presence of $NaLa(MoO_4)_2$ powders with some accumulated bulk crystals, which are composed of some small plate crystals. A few ellipsoid-like microparticles appeared when pH = 5 (Fig. 2b). On increasing the pH value to 6 (Fig. 2c), the product exhibited spherical-like microparticles still with some small plate crystals. As the pH value of the reaction system was enhanced to 7 (Fig. 2d), well dispersed uniform $NaLa(MoO_4)_2$ microspheres with an average diameter of about 1 μm were obtained. When the pH value varied from 7 to 8 (Fig. 2e), regular microspheres disappeared and three kinds of morphologies of the product coexisted: non-regular spheres, shuttle-like architectures and ellipsoid-like crystals, but they shared the same XRD pattern (Fig. 1e). The morphology changed again when the pH value of the solution was increased to 9 and the product exhibited some dissolved spheres and ellipsoid-like crystals (Fig. 2f).

The microspheres obtained with pH = 7 were further characterized by transmission electron microscopy (TEM) and the corresponding selected area electron diffraction (SAED) pattern. Fig. 3a presents a typical TEM image, from which one can clearly see that the $NaLa(MoO_4)_2$ microsphere was formed as a single particle rather than the aggregation of numerous nanocrystals. The corresponding SAED pattern (Fig. 3b) clearly indicates the mono crystalline nature of the product.

On the basis of the above discussion, our experimental results indicate that the starting pH value plays an important role in the pure-phase formation and uniform morphology of $NaLa(MoO_4)_2$ microspheres. On the one hand, the crystalline phase of the nuclei is critical for directing the intrinsic shapes of the crystals due to its characteristic symmetry and structure.[20] On the other hand, NaOH acting as the mineralizer in varying pH value, to a certain extent, would change the growth rate of crystallographic planes with different surface energies so as to form different crystallite morphologies.[21,22] Therefore, a pH value of 7 was optimal for good crystallization. To further study the formation mechanism of the microspheres, controllable experiments were carried out by adjusting the reaction time and a possible synthesis mechanism for the microspheres was proposed in the next section.

3.2. Formation mechanism for the $NaLa(MoO_4)_2$ microspheres

The crystal growth mechanisms in solution are so complicated that the actual crystallization mechanism remains an open question. The Ostwald ripening, selective polymer adsorption, and oriented attachment *etc.* were adopted to account for the process of crystal growth. In order to understand the formation process of the $NaLa(MoO_4)_2$ microspheres, we carried out time-dependent experiments during which samples were collected from the reaction mixture at different growth stages.

From the FE-SEM observations, we found that the Ostwald ripening process dominated the crystallization process at the initial stage. That is, at the initial stage tiny crystalline nuclei

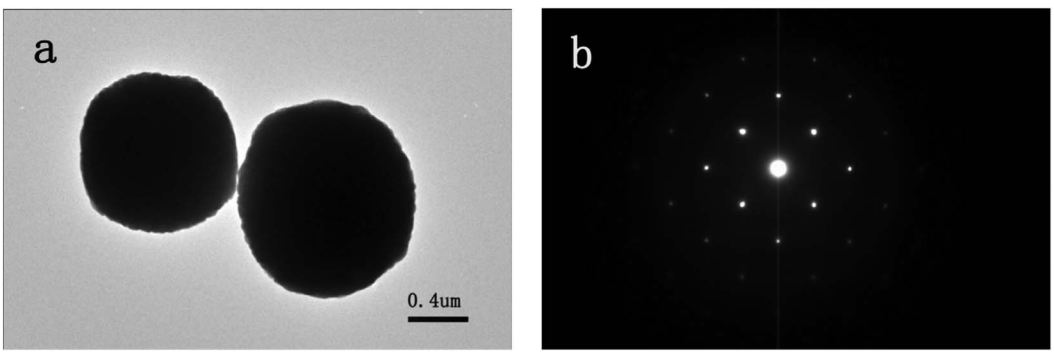

Fig. 3 (a) TEM and (b) the corresponding SAED pattern of the $NaLa(MoO_4)_2$ microspheres obtained hydrothermally at 180 °C for 12 h at pH = 7.

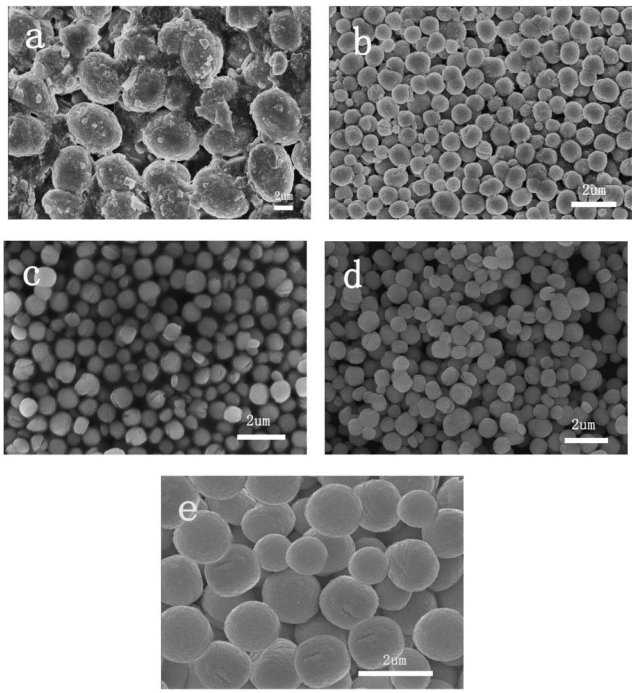

Fig. 4 FE-SEM images of the products synthesized at 180 °C and pH = 7 with different times: (a) just after the pH value of the solution was adjusted; (b) after stirring 1 h before hydrothermal treatment; (c) after hydrothermal treatment for 1 h; (d) 2 h; (e) 12 h.

form in a supersaturated solution that acts as the centers of crystallization. Then the crystal growth follows and bigger particles grow at the expense of smaller crystals, as described by the Gibbs–Thompson equation. As shown in Fig. 4a, ellipsoid-like microparticles with an average diameter of 4 μm were formed immediately after the pH value of the precipitate was adjusted to 7 before hydrothermal treatment. After the precipitate was stirred for 1 h just before being transferred to the Teflon-sealed autoclave, the obtained product exhibits a spherical-like structure with some small seeds like an aggregation, which has an average diameter of 500 nm, which was shown in Fig. 4b. When the reaction was carried out for about 1 h at 180 °C, a regular spherical-like structure remained, while the small seeds disappeared (Fig. 4c). As the reaction time was increased from 2 to 12 h, uniform microspheres were obtained, and the particle sizes increased gradually into an average diameter of 1 μm with the prolonging of the reaction time (Fig. 4d, e), indicating that the formation of the microspheres needs a certain ripe time.

On the basis of the above discussion, it has been suggested that the formation of $NaLa(MoO_4)_2$ microspheres may result from a fast crystallization–dissolution–re-crystallization growth mechanism. The process of the morphology evolution of $NaLa(MoO_4)_2$ microspheres is schematically illustrated in Scheme 1.

3.3. Luminescent properties of $NaLa_{1-x}(MoO_4)_2$:xLn^{3+} (Ln = Eu or Dy) samples

The Eu^{3+} ion is a well-known red-emitting activator in commercial phosphors because the emission of the rare earth Eu^{3+} ion consists usually of lines in the red spectral area due to the $^5D_0$–^7F_J (J = 1–6) transitions. Moreover, Eu^{3+} doped phosphors usually have an effective and intrinsic absorption due to the 4f–4f transition of Eu^{3+} at about 395 or 465 nm, which make them match well with the near-UV and blue GaN-based LED chips, respectively. Fig. 5 shows the excitation and emission spectra of the $NaLa_{0.98}(MoO_4)_2$:$0.02Eu^{3+}$ samples with different morphologies arising from different starting pH values. The excitation spectra were obtained by monitoring the emission of the Eu^{3+} $^5D_0$–$^7F_2$ transition at 616 nm. The excitation spectrum consists of a strong broad band from 200 to 350 nm with a band maximum at 286 nm, which is ascribed to the O–Mo charge-transfer (C–T) transition. The general f–f transitions within the Eu^{3+} $4f^6$ electron configuration can also be observed in the longer wavelength region (360–550 nm), and the strong excitation peaks at 395 and 465 nm are attributed to the $^7F_0$–$^5L_6$ and $^7F_0$–$^5D_2$ transitions of the Eu^{3+} ions, respectively. The emission spectrum consists of the $^5D_0$–^7F_J (J = 1, 2, 4) emission lines of the Eu^{3+} ions with the stronger emission for J = 2 at about 616 nm upon excitation at 395 nm. It is well known that Eu^{3+} is an excellent structure probe for investigating the local environment in a host lattice. In general, the magnetic-dipole-allowed $^5D_0$–$^7F_1$ transition is insensitive to the local symmetry in the crystal field (if it is dominant in the emission spectrum the Eu^{3+} ions occupy an inversion center) while the electric-dipole-allowed $^5D_0$–$^7F_2$ transition is hypersensitive to relatively small changes in the chemical surroundings of the Eu^{3+} ions (it will become the strongest one if the Eu^{3+} ion is in a site without inversion symmetry).[23,24] The emission spectra indicate that Eu^{3+} is located in an asymmetric cation environment, which is consistent with a symmetry S_4 without an inversion center. As can be seen from the emission spectra, the $NaLa_{0.98}(MoO_4)_2$:$0.02Eu^{3+}$ samples exhibit strong red emissions, which can be clearly seen from the luminescence photographs (insets of Fig. 5). Besides, one can find from the emission spectra that the red emission intensity of the product obtained at pH = 7 is the strongest among the three samples. It is clear that reduced luminescence is often observed when the excitation occurs near the surface of a phosphor, *i.e.* a surface dead layer is observed. This dead layer has been primarily attributed to surface recombination. When pH = 7, the crystallinity is clearly improved and a high density of surface states exist in the luminescent "dead layer", which will reduce the rate of surface recombination.[25] Therefore, the luminescent intensity of the product at pH = 7 is the strongest due to the influence of the reduced surface recombination. When the pH is lower than 7, the products have the spherical-like morphologies coexisting with small plate crystals and this non-uniform morphology has an important effect on the luminescent property of the products under the effect of non-radiative recombination. The same reason also can be used to explain the weak intensity of the product obtained at pH = 8.[25–27] Due to the similarity in spectral patterns, the emission spectra under 465 nm excitation were not displayed and discussed here. In summary, the uniform and well-crystallized $NaLa(MoO_4)_2$:Eu^{3+} microspheres synthesized in our experiment can be used as a red component for white light emitting diodes (W-LEDs).

The emission intensity of phosphors is also significantly affected by the concentration of activators. $NaLa_{1-x}(MoO_4)_2$:xEu^{3+} (x =

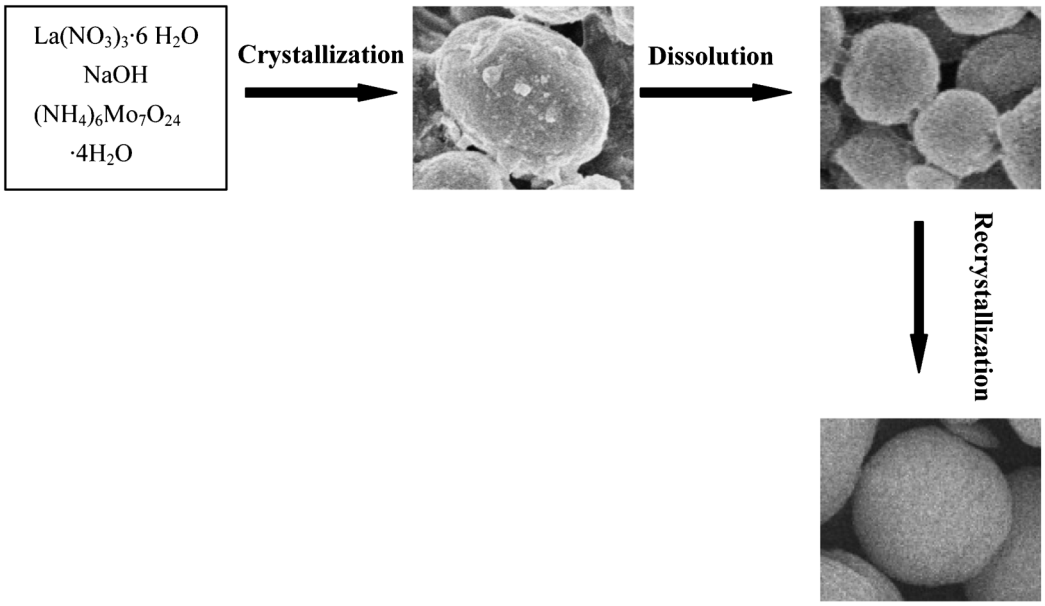

Scheme 1 Schematic illustration of the formation and morphology evolution of the $NaLa(MoO_4)_2$ microspheres in the whole synthetic process.

0.02, 0.10, 0.30, 0.50, 0.70) samples have been prepared in our experiment. The XRD patterns indicate that the phosphors are of single phase with the scheelite-type tetragonal structure, and the doped Eu^{3+} ions have little influence on the host structure (Fig. S1, ESI†). In order to determine the optimal doping concentration, the dependence of the emission intensity upon the Eu^{3+} concentration was studied under excitation at 395 nm and the results are depicted in Fig. 6. As shown in Fig. 6, a quenching concentration of 30 mol% can be observed. Usually, concentration quenching occurs because of pairing or aggregation of the identical luminescent centers at high concentration, which leads to a small average distance and efficient resonant energy transfer between Eu^{3+} ions, and a fraction of energy migration to distant killer or quenches followed by the appearance of the quenching effect. In these compounds, the bond angles of O–Mo–O and Eu–O–Mo are 105° and 100°, respectively, resulting in the long distance between Eu^{3+} ions,[28–30] which causes difficulties for energy transfer occurrence between Eu^{3+} ions. Therefore, the concentration quenching occurs at a high Eu^{3+} concentration in the $NaLa(MoO_4)_2$:Eu^{3+} powders.

The Dy^{3+} ion has also been chosen as an activator in the host $NaLa(MoO_4)_2$ since it can emit yellow and blue lights corresponding to the $^4F_{9/2}$–$^6H_{13/2}$ and $^4F_{9/2}$–$^6H_{15/2}$ transitions, respectively. The transition $^4F_{9/2}$–$^6H_{13/2}$ is hypersensitive and can be influenced by the surrounding chemical environment of the Dy^{3+} ions in the host lattice, so at a suitable lattice site, white light emitting can be fulfilled by the two color light emissions of Dy^{3+} ions.[31,32] Fig. 7 displays the excitation and emission spectra of the $NaLa_{0.98}(MoO_4)_2$:$0.02Dy^{3+}$ microspheres. The excitation spectrum was obtained by monitoring the emission of the Dy^{3+}

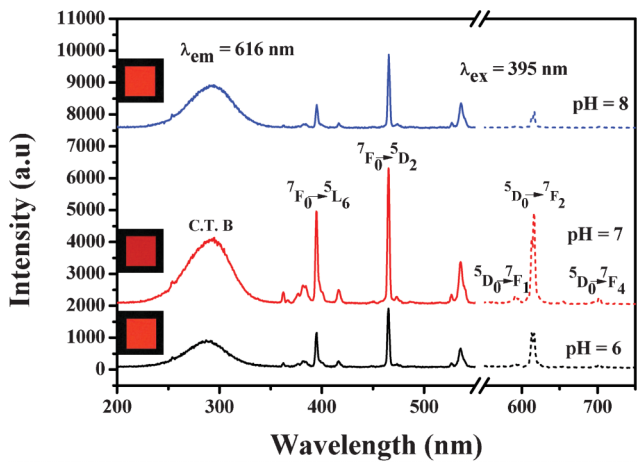

Fig. 5 PL excitation and emission spectra of $NaLa_{0.98}(MoO_4)_2$:$0.02Eu^{3+}$ samples prepared hydrothermally at 180 °C for 12 h from different starting pH values. The insets are the corresponding luminescence photographs of the samples upon excitation at 254 nm with a UV lamp.

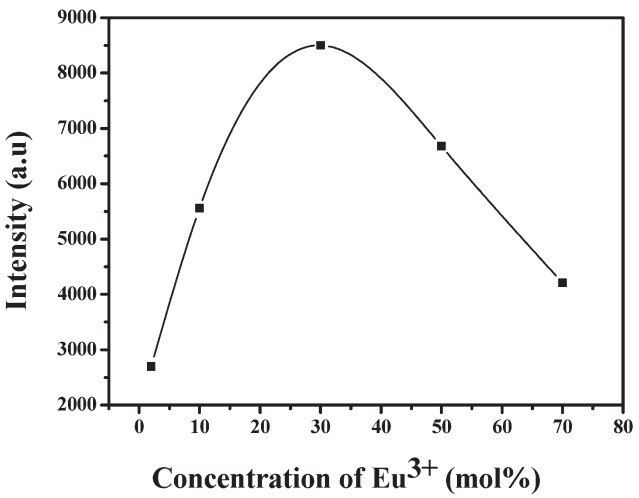

Fig. 6 Relationship between the luminescence intensity of $NaLa_{1-x}(MoO_4)_2$:xEu^{3+} (x = 0.02, 0.10, 0.30, 0.50, 0.70) microspheres and the concentration of Eu^{3+} ions (x).

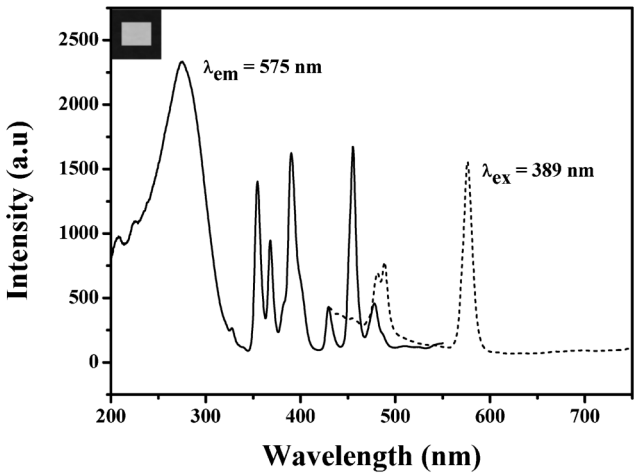

Fig. 7 PL excitation and emission spectra of $NaLa_{0.98}(MoO_4)_2$:$0.02Dy^{3+}$ microspheres prepared hydrothermally at 180 °C for 12 h from starting pH = 7. The inset is the corresponding luminescence photograph of the sample upon excitation at 254 nm with a UV lamp.

$^4F_{9/2}$–$^6H_{13/2}$ transition at 575 nm. The excitation spectrum consists of a strong broad band from 200 to 350 nm with a maximum at 274 nm, which is ascribed to the O–Mo charge-transfer (C–T) transition, and the strong excitation peaks at 389 and 455 nm. Upon the excitation at 389 nm, the emission spectrum exhibits sharp peaks at 487 and 575 nm, corresponding to the $^4F_{9/2}$–$^6H_{15/2}$ and $^4F_{9/2}$–$^6H_{13/2}$ transitions, respectively. The forced electric dipole transition $^4F_{9/2}$–$^6H_{13/2}$ transition ($\Delta J = 2$) is hypersensitive to the chemical environment around the Dy^{3+} ions in the host lattice. The emission spectrum exhibits the stronger emission for $^4F_{9/2}$–$^6H_{13/2}$ transition, indicating that Dy^{3+} ions are located at low-symmetry sites with no inversion centers in the $NaLa(MoO_4)_2$ microspheres, which are consistent with the emission spectrum of the $NaLa_{0.98}(MoO_4)_2$:$0.02Eu^{3+}$ microspheres. The emission color was also analyzed and confirmed with the help of Commission Internationale de l'Eclairage (CIE) chromaticity coordinates. The CIE chromaticity coordinate for the $NaLa_{0.98}(MoO_4)_2$:$0.02Dy^{3+}$ phosphor under 389 nm excitation is located at ($x = 0.317$, $y = 0.328$). It is obvious that the coordinate is very close to the standard white illuminate (0.333, 0.333). The color temperature for the $NaLa_{0.98}(MoO_4)_2$:$0.02Dy^{3+}$ phosphor is 6802 K, which is close to the standard color temperature of white light (6500 K). As can be seen clearly from the luminescence photograph (inset of Fig. 7), the $NaLa_{0.98}(MoO_4)_2$:$0.02Dy^{3+}$ phosphor exhibits strong white emission. Therefore, the $NaLa(MoO_4)_2$:Dy^{3+} microspheres is a promising white light-emitting phosphor, which is well matched with the near-UV LED chips.

4. Conclusion

In summary, uniform and well-crystallized $NaLa(MoO_4)_2$ microspheres with an average diameter of 1 μm have been successfully synthesized by a facile hydrothermal method without using any templates. A pH value of 7 was optimal for the crystallization of $NaLa(MoO_4)_2$ microspheres with pure-phased uniform morphology. Our experimental results indicated that the formation of microspheres was dominated by a fast crystallization–dissolution–re-crystallization growth mechanism. The luminescent properties of Eu^{3+} and Dy^{3+} ions in $NaLa(MoO_4)_2$ microspheres were also investigated. The results demonstrated that $NaLa_{1-x}(MoO_4)_2$:xLn^{3+} (Ln = Eu or Dy) microspheres exhibited good luminescent properties and might have potential applications in lighting technology. However, further work is underway to study the intrinsic physical properties of the well prepared samples and the possibility of synthesizing other related inorganic compounds.

Acknowledgements

This work was supported by the National Science Foundation of China (no. 11004081), partially supported by the Science and Technology Innovation Projects of Jilin Province for overseas students and by the Open Project of State Key Laboratory of Rare Earth Resources Utilization, Changchun Institute of Applied Chemistry, Chinese Academy of Sciences (RERU2011005).

References

1 D. D. Archibald and S. Mann, *Nature*, 1993, **364**, 430.
2 A. P. Alivistos, *Science*, 1996, **271**, 933.
3 Z. H. Xu, C. X. Li, P. P. Yang, C. M. Zhang, S. S. Huang and J. Lin, *Cryst. Growth Des.*, 2009, **9**, 4752.
4 X. D. Wang, J. H. Song, J. Liu and Z. L. Wang, *Science*, 2007, **316**, 102.
5 S. J. Chen, Y. C. Liu, C. L. Shao, R. Mu, Y. M. Lu, J. Y. Zhang, D. Z. Shen and X. W. Fan, *Adv. Mater.*, 2005, **17**, 586.
6 L. Zhang, D. R. Chen and X. L. Jiao, *J. Phys. Chem. B*, 2006, **110**, 2668.
7 J. Yang, Z. W. Quan, D. Y. Kong, X. M. Liu and J. Lin, *Cryst. Growth Des.*, 2007, **7**, 730.
8 G. Blasse, *Chem. Mater.*, 1994, **6**, 1465.
9 A. A. Kaminskii, *Crystalline Lasers: Physical Processes and Operating Schemes*, CRC Press, Boca Raton, FL, 1996.
10 D. B. Barber, C. R. Pollock, L. L. Beecroft and C. K. Ober, *Opt. Lett.*, 1997, **22**, 1247.
11 Y. R. Do and Y. D. Huh, *J. Electrochem. Soc.*, 2000, **147**, 4385.
12 S. Neeraj, N. Kijima and A. K. Cheetham, *Chem. Phys. Lett.*, 2004, **2**, 387.
13 L. Y. Zhou, L. H. Yi, R. F. Sun, F. Z. Gong and J. H. Sun, *J. Am. Ceram. Soc.*, 2008, **91**, 3416.
14 C. F. Guo, S. T. Wang, T. Chen, L. Luan and Y. Xu, *Appl. Phys. A: Mater. Sci. Process.*, 2009, **94**, 365.
15 C. P. Grey, C. M. Dobson, A. K. Cheetham and R. J. B. Jakeman, *J. Am. Chem. Soc.*, 1989, **111**, 505.
16 B. J. Kennedy, B. A. Hunter and C. J. Howard, *J. Solid State Chem.*, 1997, **130**, 58.
17 D. Boyer, G. Bertrand-Chadeyron, R. Mahiou, C. Caperaa and J.-C. Cousseins, *J. Mater. Chem.*, 1999, **9**, 211.
18 M. K. Jung, W. J. Park and D. H. Yoon, *Sens. Actuators, B*, 2007, **126**, 328.
19 H. M. Cheng, J. M. Ma, Z. G. Zhao and L. M. Qi, *Chem. Mater.*, 1995, **7**, 663.
20 D. Chen, K. B. Tang, F. Q. Li and H. G. Zheng, *Cryst. Growth Des.*, 2006, **6**, 247.
21 S. H. Yu, B. Liu, M. S. Mo, J. H. Huang, X. M. Liu and Y. T. Qian, *Adv. Funct. Mater.*, 2003, **13**, 639.
22 C. Jia, Y. Cheng, F. Bao, D. Q. Chen and Y. S. Wang, *J. Cryst. Growth*, 2006, **294**, 353.
23 Z. L. Wang, H. B. Liang, M. L. Gong and Q. Su, *Opt. Mater.*, 2007, **29**, 896.
24 M. F. Zhang, H. Fan, B. J. Xi, X. Y. Wang, C. Dong and Y. T. Qian, *J. Phys. Chem. C*, 2007, **111**, 6652.
25 B. L. Abrams and P.H. Holloway, *Chem. Rev.*, 2004, **104**, 5783.
26 Y. H. Zheng, H. P. You, G. Jia, K. Liu, Y. H. Song, M. Yang and H. J. Zhang, *Cryst. Growth Des.*, 2009, **9**, 51.

27 V. Sudarsan, F. C. J. M. van Veggel, R. A. Herring and M. Raudsepp, *J. Mater. Chem.*, 2005, **15**, 1332.
28 C. Guo, B. Li and F. Jin, *J. Lumin.*, 1991, **12**, 118–126.
29 C. H. Chiu, C. H. Liu, S. B. Huang and T. M. Chen, *J. Electrochem. Soc.*, 2008, **155**, J71–J78.
30 D. L. Dexter and H. J. Schulman, *Chem. Phys.*, 1954, **22**, 1063–1070.
31 Q. Su, H. B. Liang, C. Y. Li, H. He, Y. H. Lu, J. Li and Y. Tao, *J. Lumin.*, 2007, **927**, 122–123.
32 W. C. Lü, H. Zhou, G. T. Chen, J. F. Li, Z. J. Zhu, Z. Y. You and C. Y. Tu, *J. Phys. Chem. C*, 2009, **113**, 3844.